Liquid Crystals
Publication details, including instructions for authors and subscription information:
http://www.informaworld.com/smpp/title~content=t713926090

Optimal pixel design for low driving, single gamma curve and single cell-gap transflective fringe-field switching liquid crystal display

Youn Hak Jeong[a]; Young Jin Lim[a]; Eun Jeong[a]; Won Gun Jang[b]; Seung Hee Lee[b]
[a] Polymer BIN Fusion Research Center, School of Advanced Materials Engineering, Chonbuk National University, Chonju, Chonbuk 561-756, Korea [b] Korea Photonics Technology Institute, Wolchul-dong, Buk-gu, Gwangju 500-460, Korea

To cite this Article Jeong, Youn Hak , Lim, Young Jin , Jeong, Eun , Jang, Won Gun and Lee, Seung Hee(2008) 'Optimal pixel design for low driving, single gamma curve and single cell-gap transflective fringe-field switching liquid crystal display', Liquid Crystals, 35: 2, 187 — 194
To link to this Article: DOI: 10.1080/02678290701790911
URL: http://dx.doi.org/10.1080/02678290701790911

Liquid Crystals,
Vol. 35, No. 2, February 2008, 187–194

Taylor & Francis
Taylor & Francis Group

Optimal pixel design for low driving, single gamma curve and single cell-gap transflective fringe-field switching liquid crystal display

Youn Hak Jeong[a], Young Jin Lim[a], Eun Jeong[a], Won Gun Jang[b] and Seung Hee Lee[b]*

[a]*Polymer BIN Fusion Research Center, School of Advanced Materials Engineering, Chonbuk National University, Chonju, Chonbuk 561-756, Korea;* [b]*Korea Photonics Technology Institute, Wolchul-dong, Buk-gu, Gwangju 500-460, Korea*

(Received 15 October 2007; accepted 6 November 2007)

When a dielectric layer, in-cell retarder (ICR) is formed between the electrode and LC layer to obtain a single-gap transflective fringe-field switching (FFS) display, the driving voltage is highly increased due to the thickness of the dielectric material. In particular, the driving voltage of the transmissive part becomes very high, and goes beyond the driver integrated circuit (IC) range for mobile application because the homogenously aligned liquid crystal director should rotate twice as far as that in the reflective part. The correlation between the driving voltage and electrode structures was investigated. It was found that the problem could be solved by optimisation of the common electrode structure such that the electrode structure changed from a plane to slit shape (in-plane field is mainly used instead of fringe field), realising a high performance FFS transflective display.

Keywords: liquid crystal display; transflective; fringe-field switching; in-cell retarder

1. Introduction

For portable electronic devices, transflective liquid crystal displays (LCDs) have been developed due to their excellent visible quality under any environmental lighting conditions, while maintaining characteristics, such as portability, good legibility and low power consumption (*1*). Basically, as the reflective part of a transflective LCD has a double light path compared with the transmissive part, a phase retardation discrepancy is caused between these two parts. Therefore, until now, this problem was solved using a commercial dual cell-gap transflective display. However, this device has associated manufacturing process and display qualities problems.

To overcome these issues, single cell-gap transflective LCDs have been widely studied. Among the various structures proposed using different liquid crystal modes, extensive studies have been performed (*2–9*) on the fringe-field switching (FFS) mode, where the homogenously aligned liquid crystals are rotated by a fringe electric field, because the FFS mode exhibits excellent performance in terms of electro-optical characteristics in transmissive displays (*10–16*).

According to a previous report, an in-cell retarder (ICR) is required for a transflective FFS device to exhibit excellent electro-optical properties (*6*). In general, a thickness of the ICR layer of about 1 μm is required to give rise to a retardation value of a quarter-wave plate due to its limited birefringence. Therefore, when an ICR layer is placed between the FFS array and LC layer, it causes a rapid increase in the operating voltage (V_{op}), since an average twisted angle of LC director from its initial orientation in the transmissive part should be 45°, which will exceed the driver integrated circuit (IC) range for mobile application. To solve this issue, slit angles, defined as the angle between the horizontal field direction and the initial LC director in the transmissive and reflective parts, were adjusted, respectively, to change the V_{op}, although the results were not satisfactory (*4, 5*).

To remove the increase in the V_{op}, the ICR layer was placed on the bottom substrate, with a colour filter and reflector, with the FFS array positioned on top of the substrate (*6–9*); however, in such a case, an active layer made of amorphous silicon in the thin film transistor part is exposed to environmental light, which will cause severe photocurrent leakage, leading to the degradation of the display qualities, such as strong flicker, cross-talk and image sticking level (*17*). Another cell structure, where the patterned ICR layer was placed below the top colour filter substrate in the reflective part of the sub-pixel area, with the array substrate and reflector placed on the bottom substrate in the reflective part has been proposed (*18–20*). In this case, the V_{op} of the transmissive part in the transflective mode was able to be set as low as that in the transmissive mode. In this structure, the patterned ICR in the reflective part has a retardation of a half-wave plate ($\lambda/2$); therefore, the retardation of the LC layer should be a quarter-wave plate ($\lambda/4$) to achieve a good dark state. Since the retardation of the LC layer in the transmissive area should be larger

*Corresponding author. Email: lsh1@chonbuk.ac.kr

ISSN 0267-8292 print/ISSN 1366-5855 online

DOI: 10.1080/02678290701790911
http://www.informaworld.com

than $\lambda/2$ to maximize light efficiency in the FFS mode (*21*), a dual cell-gap structure is absolutely required to maximize the light efficiency in both the transmissive and reflective parts. The problem of the proposed structure is that the dark state in the reflective part is so sensitive to change in the retardation value of the ICR and LC layer; in addition, there is a manufacturing issue in relation to a dual cell gap, which might cause non-uniformity in the LC orientation and rubbing.

In this paper, a transflective FFS LCD with a single cell gap and single gamma is proposed. Since the ICR on the bottom array substrate causes mismatch between the voltage–transmittance (V–T) and voltage–reflectance (V–R) curves, the correlation between V_{op} and the electrodes structures was analysed, and a new optimised electrode structure for the transmissive and reflective parts proposed for the single-gamma transflective FFS display. The detailed electro-optical characteristics are also described.

2. Cell structure and switching principle of single cell-gap FFS transflective LCD

Figure 1 a shows a cross-sectional view of the proposed cell structure. Here, each common and pixel electrode in the transmissive part is made of slit-type transparent material. In the reflective part, a common electrode is made of plane-type reflective metal, and a pixel electrode of slit type transparent material. An ICR with a quarter wave plate ($\lambda/4$) exists below the LC layers, but on the pixel electrode layer. As shown in Figure 1 b, the optical axis of the LC layer is aligned parallel to the analyser, but at 45° with respect to the optical axis of the ICR in the reflective part. In the transmissive part, another compensation film, with a quarter wave plate, exists at an angle of 90° with respect to optical axis of the ICR. In this way, both the transmissive and reflective parts show a dark state before application of a voltage (*6*). Of course, when the ICR is patterned to exist only in the reflective part, the quarter wave film below the bottom substrate is not necessary.

The transmittance, T, and reflectance, R, of the FFS transflective display can be described as follows (*22*):

$$T = \frac{1}{2}\sin^2 2(\chi \pm \alpha)\sin^2\frac{\Gamma}{2} \quad \text{(crossed polarisers)} \quad (1)$$

$$R = \frac{1}{2}\sin^2 4(\chi \pm \alpha)\sin^2\frac{\Gamma}{4}, \quad (2)$$

where χ is the ideal twist angle relative to the transmission axis of the polariser, α is the over-twisted or under-twisted angle due to sufficiently or inadequately applied field and γ is the phase retardation of the LC cell. To maximise T and R, the rotation angle of the LC director in the transmissive and reflective parts should be 45° and 22.5° with $\alpha = 0°$, respectively. From equations (1)–(2), one can notice that the existence of α will cause transmittance decrease by 2α in the transmissive region and, in addition, will be decreased by 4α in the reflective region. In other words, if the voltage-dependent transmittance and reflectance curves are not well matched, the light efficiency of the device will be very poor. Nevertheless, the advantage of the device is that the dark state of the reflective part is independent of the thickness of the LC layer (*6*).

As one of the commercial ICR materials has a birefringence value of about 0.15, the ICR has to have a thickness of about 900 nm to obtain a phase retardation of $\lambda/4$. This thick dielectric material increases the operating voltage with decreasing electric field strength in the LC layer. In this study, analyses of the relationships between the ICR thickness on the electrode layers and the electro-optical properties were deeply carried out in detail. An LC with the following physical parameters was used: birefringence $\Delta n = 0.1$; dielectric anisotropy $\Delta\varepsilon = 8.2$; elastic constants $K_1 = 9.7$ pN, $K_2 = 5.2$ pN, $K_3 = 13.3$ pN. The surface tilt angle of the LC was 2°, with an initial rubbing direction of 83° with respect to horizontal component of a fringe electric field. The cell gap was 3.8 μm. The transmittances of the single and parallel polarisers were assumed to be 43 and 37%, respectively.

3. Results and discussion

In a typical FFS mode, the common and pixel electrodes have to be placed in the same array substrate to generate a fringe electric field, with both composed of transparent electrodes such as indium–tin oxide (ITO). In this paper, the first and second ITOs play the roles of common and pixel electrode, respectively. There are two ways of a generating a fringe field such that the shape of the common electrode can be in the form of both plane and slit (*10*).

For this study, a plane shape was chosen for the common electrode in the reflective part with the width (w) of the pixel electrode and the distance (l') between them optimized to realise a single gamma circuit with high light efficiency, as shown in Figure 2. In the transmissive part, the common electrode is patterned in a slit form and, thus, the

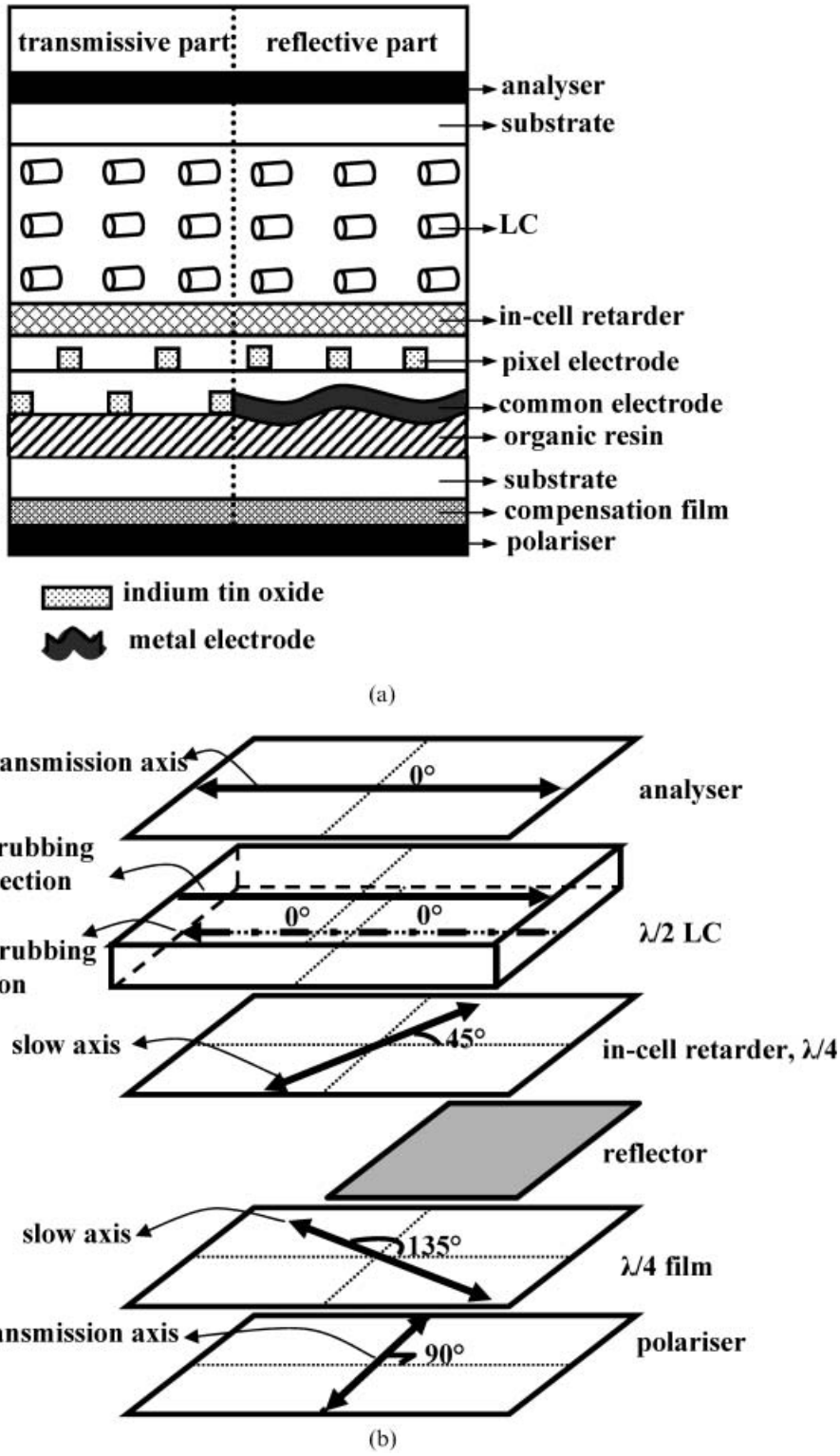

Figure 1. (a) Cross-sectional view and (b) optical configuration of the single cell-gap transflective FFS LCD.

electrode width and the distance (l) between the pixel and common electrode were investigated. One interesting area is that when a dielectric material, such as an ICR layer, stacks highly up on the electrode layers, considerably, different behaviour in the increase of the V_{op} and maximum transmittance (T_{max}) (defined as the average light efficiency generated in a repeatable electrode unit including pixel and common

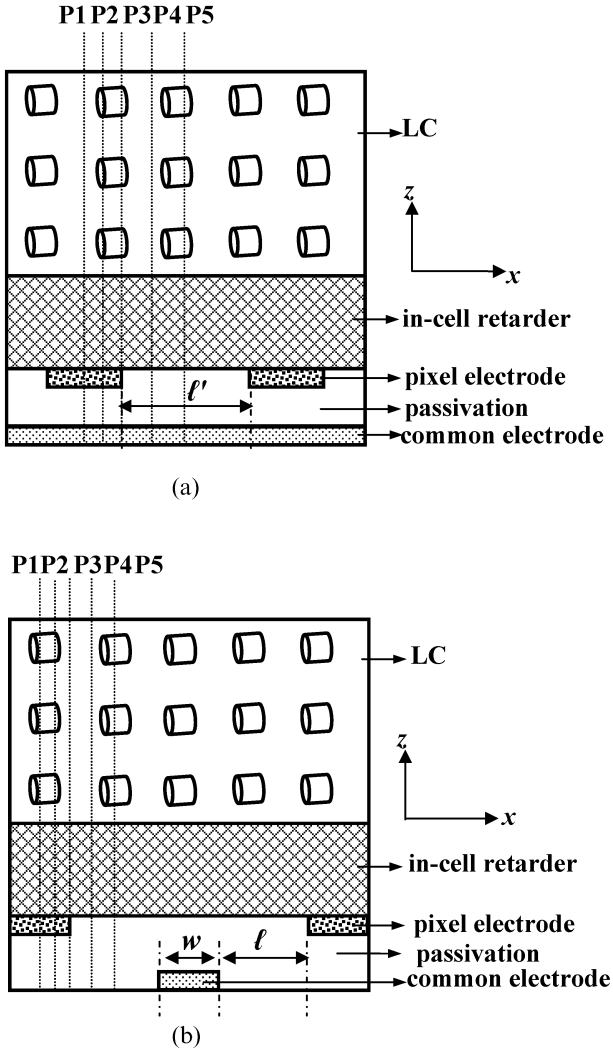

Figure 2. Detailed electrode structure with (a) plane and (b) slit-shaped common electrodes.

electrodes at V_{op} i.e. distances $w+l'$ and $w+l$ for a plane and a slit-shape common electrode, respectively) between the above two cases were observed.

Figure 3 shows how V_{op} and T_{max} change according to the thickness of the ICR for two different structures. For these calculations, w was 3 µm and l' was 5 µm in the plane type and w and l were both 4 µm in the slit type. The passivation layer had a thickness and dielectric constant (ε) of 200 nm and of 6.5, respectively, whereas the thickness of the ICR with $\varepsilon=5$ was varied from 100 nm to 900 nm to obtain V_{op} and T_{max}. As expected, V_{op} increased with increasing thickness of the ICR; however, the increasing level of the V_{op} totally depended on the structure of the first ITO layer, whether it was either plane or slit. As the ICR thickness was increased from 100 nm to 900 nm, V_{op} of the electrode structure composing of the plane plate was greatly

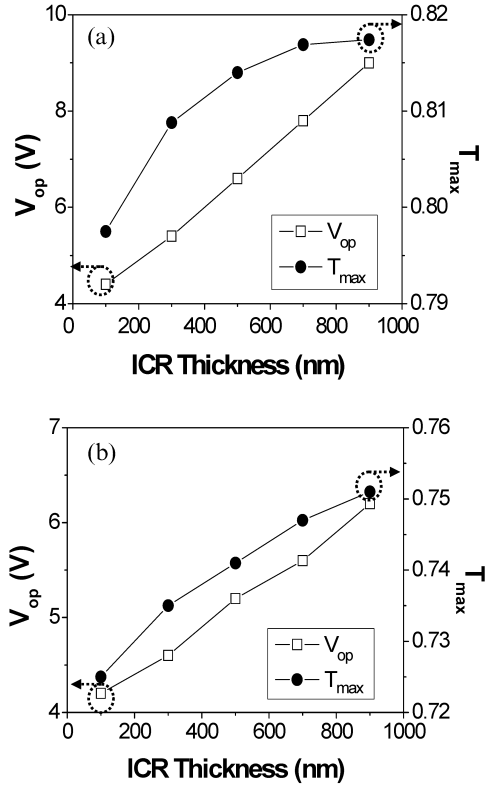

Figure 3. Operation voltage and maximum transmittance as a function of the ICR thickness with (a) plane and (b) slit-shaped common electrodes.

increased from 4.4 to 9 V, but only increased from 4.2 to 6.2 V in the slit type. One interesting fact is that T_{max} also increases slightly with increasing ICR thickness.

In order to achieve a competitive single-gap and single-gamma transflective LCD with good electro-optical performances, such as high light efficiency and low V_{op}, and at low cost, the two properties associated with driving issues should be satisfied. Initially, a condition in which both voltage-dependent transmittance and reflectance curves match is required, so that a single gamma curve is used for low cost. Secondly, a solution for a low V_{op} in the transmissive part needs to be found, so that the display can be driven using a conventional mobile driver IC. From this perspective, a slit-type common electrode was chosen in the transmissive part.

In addition, in order to understand the increase of T_{max}, we calculated the light efficiency along electrodes in relation to the ICR thickness for plane and slit-shaped electrodes, as shown in Figure 4. One interesting fact is that the light efficiency at most electrode positions, except for the edge of pixel electrode, P3, increases, especially in and close to the P1 and P5 regions, which are at the centres of the pixel and common electrodes in relation to the

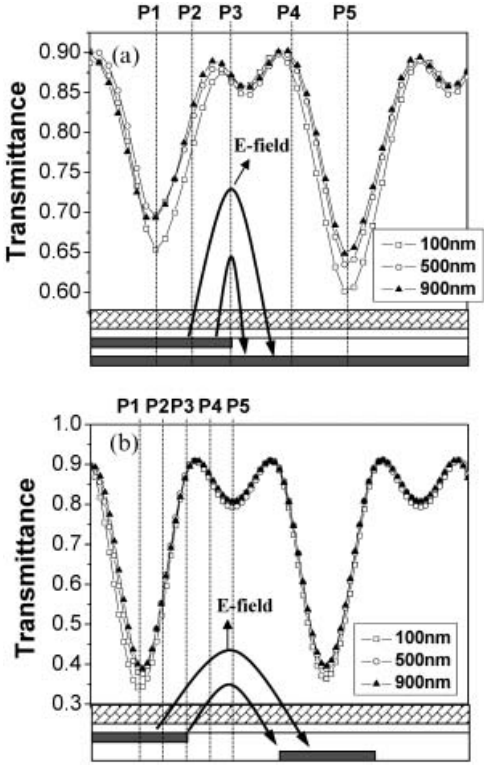

Figure 4. Transmittance curves in relation to the ICR thickness with (a) plane and (b) slit-shaped common electrodes.

ICR thickness in a plane structure, as shown in Figure 4 a. On the other hand, the light efficiency in a slit structure increases slightly only at the electrode positions of P1 and P2, which are in the centre and close to that in the slit electrodes, but the light efficiency in the other regions remains the same despite the great increase in the operating voltage, as shown in Figure 4 b. From both results, one can understand that the slight increase in T_{max} comes mainly from increase in light efficiency around the centre of both pixel and common electrodes.

To thoroughly analyse voltage in relation to the ICR thickness of the two different common electrode shapes, the voltage, V, and electric field strength, E, in the LC layer over the electrode were calculated using numerical formulae described as follows:

$$\mathrm{V} = \int E d\ell,\ d\ell = (dx + dz), \tag{3}$$

$$dV = \frac{\partial V}{\partial x}dx + \frac{\partial V}{\partial z}dz, \tag{4}$$

$$dV = E_x dx + E_z dz,\ \left(E_x = \frac{\partial V}{\partial x},\ E_z = \frac{\partial V}{\partial z}\right). \tag{5}$$

Equation (3) shows the relationship between voltage and electric field strength. Generally, $d\ell$ can be defined by $d_x+d_y+d_z$, but the simulator used in this study, which was the commercially available software "LCD master" (Shintech, Japan), provides only two dimensions composed of d_x and d_z. When equation (3) is differentiated, equation (4) can be obtained, which alternatively can be expressed as equation (5). In equation (5), if the z-directional (vertical) vector is disregarded (d_z=0), the x-directional (horizontal) electric field strength, E_x, can be extracted and, likewise, the z-directional electric field strength, E_z, can be obtained. In the FFS device, E_x contributes to rotation of the LC director, whereas E_z contributes to tilting of the LC director (*23*).

Figure 5 shows the V_{op} and effective voltage induced in the whole LC layer when V_{op} is applied to the electrodes over the electrode positions in relation to ICR thickness. The effective voltage in the LC layer is lower than the V_{op}, as a large voltage drop occurs at thick dielectric layers between the electrode layer and LC layer. As indicated in Figure 5 a, the dropping rate of V_{op} in the LC layer at P1 is somewhat larger in the plane type such that the voltage drops from 9 V (4.4 V) to 5.2 V (2.8 V) for ICR thickness of 900 nm (100 nm). However, for the slit-shape common electrodes, it drops from 6.2 V (4.2 V) to 4.1 V (3.2 V) for ICR thickness of 900 nm

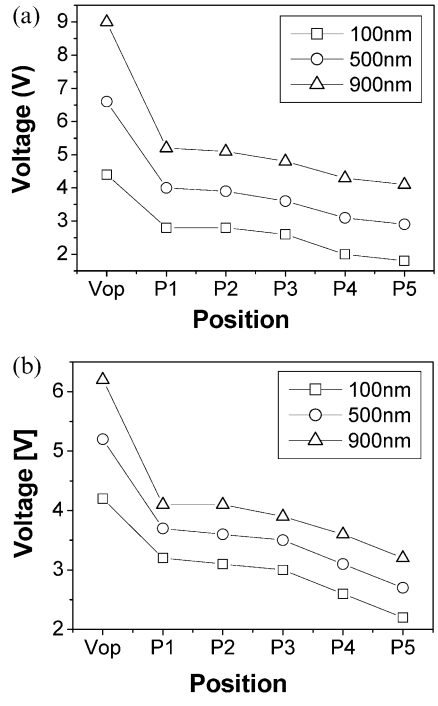

Figure 5. The V_{op} and effective voltage of the LC layer at electrode positions with (a) plane and (b) slit-shaped electrodes in relation to the ICR thickness in the transmissive area.

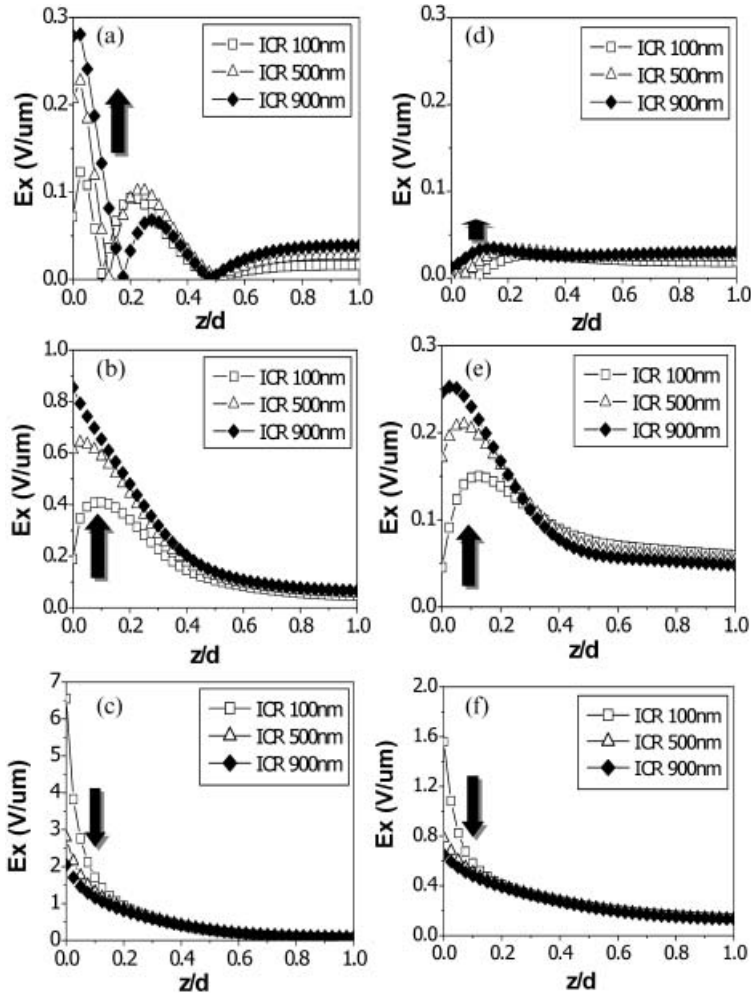

Figure 6. Horizontal field strength as a function of z/d in relation to the ICR thickness at electrode positions: (a) P1, (b) P2, (c) P3 with plane-shaped electrode and (d) P1, (e) P2, (f) P3 with a slit-shaped electrode.

(100 nm), as shown in Figure 5 b, indicating that the dropping ratio of applied voltage in the LC layer is much smaller in the slit than in the plain structure. In addition, the rate of increase in V_{op} and effective voltage with increasing ICR thickness is much smaller in the slit than in the plain structure. This behaviour might be understood from the difference in electrode structure. In other words, for a plane structure, the field line coming from the pixel electrode converges to the common electrode in the bottom layer, forming a fringe electric field line, whereas the field line is formed between pixel and common electrodes forming in-plane electric field relatively in the slit structure (see Figure 4). This implies that field strength E_x becomes weaker much easily in the plane than in the slit structure as a vertical position z is away from bottom electrode surface so that increasing thickness of ICR layer will reduce effective voltage induced in the LC layer more rapidly in the plane than in the slit structure.

In order to confirm the assertion above, E_x was calculated via differentiation of the voltage in the LC layer in two electrode structure types, as shown in Figure 6. Figures 6 a–6 c show E_x at positions P1–P3 of the plane type, whereas Figures 6 d–6 f show E_x in the P1–P3 positions of the slit type. From the E_x shown in the Figure 6, the field strength at P1 is almost negligible in both structures since it is a sink point. The greater the ICR thickness, the higher the E_x in the low region of $z/d=0.4$ at P2 occurs with the plane type, but that at P3 unexpectedly decreases, as shown in Figures 6 b and 6 c. One interesting fact is that the strength of E_x decreases rapidly away from the electrode surface and its decreasing ratio is much larger in the plane than in the slit structure, as shown in Figures 6 e and 6 f, which explains the lower increase in V_{op} in the slit structure with increasing the ICR thickness.

Figure 7 a shows voltage-dependent transmittance (V–T) curves in relation to the electrode structures of the first common electrode, such as

plane or slit types, in the transmissive part. For these calculations, a rubbing angle (RA) of 83° with respect to a horizontal component of the fringe electric field and ICR thickness of 900 nm were used. Other electrode conditions were the same as those used in Figure 3. As indicated, when the common electrode was changed from a plane to slit type, the V_{op} dramatically decreased with a slight drop in the transmittance. It was also noticeable that under the 6 V range, the slit-type device showed higher transmittance than that with the plane type. Figure 7 b shows the voltage-dependent reflectance (V–R) as a function of RA, as well as V–T curves when the common electrode had a plane shape. In the FFS mode, the shape of voltage-dependent curves was strongly dependent on RA (*8*), such that as RA decreases from 75° to 45° the V_{op} increased from 4 V to 9 V. When the V_{op} reached 9 V in the reflective part, the V–T and V–R curves could be matched with the plane shape of the common electrode. However, a V_{op} of about 9 V is too high to be driven by a mobile drive IC; therefore, the first common electrode should be composed of the slit type instead of the plane type, as the increasing rate of V_{op} in ratio to the ICR thickness is less with the slit than the plane type.

As shown in Figure 8, the V–T and V–R curves were well matched to be controlled by a single gamma

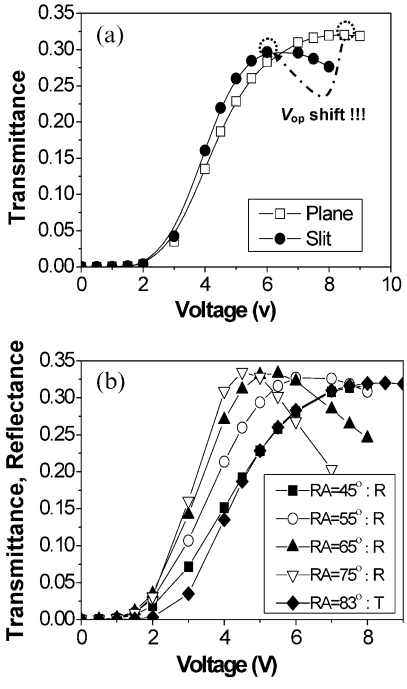

Figure 7. (a) Voltage-dependent transmittance curves in relation to the electrodes structure. (b) Voltage-dependent reflectance and transmittance curves as a function of the rubbing angles.

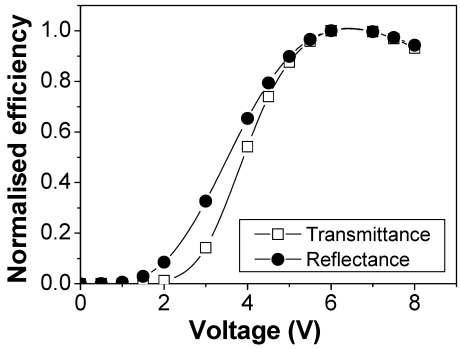

Figure 8. Voltage-dependent normalised transmittance and reflectance curves under optimum conditions.

curve when the common electrode was composed of the slit type in the transmissive part and the plane type in the reflective part. The RA of the reflective part was adjusted to 55° to match similarly to the V_{op} level of the transmissive part, which has a rubbing angle of 83°.

4. Conclusion

Summarising the features of the newly proposed single-gap transflective LCD, although the ICR layer was placed between the electrodes and LC layer, the device can realise a single driving circuit and gamma curve, and the V_{op} of the transmissive part was sufficiently low to be driven by a mobile driver IC. Furthermore, the electrode structure of the reflective part was the same as that of the existing FFS mode, with only the rubbing angle needing to be slightly adjusted to match the V–R and V–T curves.

Acknowledgements

This work was supported by Grant No R01-2004-000-10014-0 from the Basic Research Program of the Korea Science & Engineering Foundation.

References

(1) Watanabe R.; Tomita O. In *Proceedings of the 9th International Display Workshop*; Hiroshima, Japan; Dec. 4–6 2002; p 397.
(2) Jung T.B.; Song J.H.; Seo D.S.; Lee S.H. *Jap. J. appl. Phys.* **2004**, *43*, 1211–1213.
(3) Song J.H.; Lee S.H. *Jap. J. appl. Phys.* **2004**, *43*, 1130–1132.
(4) Jeong Y.H.; Kim H.Y.; Park J.B.; Kim M.S.; Kim G.H.; Seen S.M.; Lim D.H.; Kim S.Y.; Lim Y.J.; Lee S.H. *SID 05 Dig.* **2005**, 723–725.
(5) Park J.B.; Kim H.Y.; Jeong Y.H.; Lim D.H.; Kim S.Y.; Lim Y.J. *Jap. J. appl. Phys.* **2005**, *44*, 6701–6702.
(6) Song J.H.; Lim Y.J.; Lee M.-H.; Lee S.H.; Shin S.T. *Appl. Phys. Lett.* **2005**, *87*, 011108–011110.
(7) Choi M.O.; Song J.H.; Lim Y.J.; Kim T.H.; Lee S.H. *SID 05 Dig.* **2005**, 719–721.

(8) Lim Y.J.; Jeong Y.H.; Choi M.O.; Jang W.G.; Lee S.H. *Jap. J. appl. Phys.* **2005**, *44*, L1532–1534.
(9) Lim Y.J.; Lee M.H.; Lee G.D.; Jang W.G.; Lee S.H. *J. Phys. D* **2007**, *40*, 2759–2764.
(10) Lee S.H.; Lee S.L.; Kim H.Y. *Appl. Phys. Lett.* **1998**, *73*, 2881–2883.
(11) Lee S.H.; Lee S.L.; Kim H.Y.; Eom T.Y. *SID 99 Dig.* **1999**, 202–205.
(12) Lee S.H.; Lee S.M.; Kim H.Y.; Kim J.M.; Hong S.H.; Jeong Y.H.; Park C.H.; Choi Y.J.; Lee J.Y.; Koh J.W., et al. *SID 01 Dig.* **2001**, 484–487.
(13) Kondo K. *SID 05 Dig.* **2005**, 978–981.
(14) One K.; Imajo Y.; Mori I.; Oke R.; Kato S.; Endo K.; Ishino H.; Ooishi Y. *SID 05 Dig.* **2005**, 1848–1851.
(15) One K.; Mori I.; Ishii M.; Ooishi Y.; Furuhashi T. *SID 06 Dig.* **2006**, 1954–1957.
(16) Aoki N.; Komura S.; Furuhashi T.; Adachi M.; Itou O.; Miyazawa T.; Ohkura M. *J. SID* **2007**, *15*, 23–29.
(17) Yamaji Y.; Ikeda M.; Akiyama M.; Endo T. *Jap. J. appl. Phys.* **1999**, *38*, 6202–6206.
(18) Itou O.; Hirota S.; Tanno J.; Morimoto M.; Igeta K.; Imayama H.; Komura S.; Nagata T. In *Proceedings of the 13th International Display Workshop; Ostu, Japan; Dec. 6–8* 2006; p 635–638.
(19) Imayama H.; Tanno J.; Igeta K.; Morimoto M.; Komura S.; Nagata T.; Itou O.; Hirota S. *SID 07 Dig.* **2007**, 1651–1654.
(20) Hirota S.; Oka S.; Itou O.; Igeta K.; Morimoto M.; Imayama H.; Komura S.; Nagata T. *SID 07 Dig.* **2007**, 1661–1664.
(21) Jung S.H.; Kim H.Y.; Song S.H.; Kim J.H.; Nam S.H.; Lee S.H. *Jap. J. appl. Phys.* **2004**, *43*, 1028–1031.
(22) Yen P.; Gu C. *Optics of Liquid Crystal Displays*; John Wiley & Sons: Chichester, 1999; p 213–222.
(23) Hong S.H.; Park I.C.; Kim H.Y.; Lee S.H. *Jap. J. appl. Phys.* **2000**, *39*, L527–L530.